

Friction-induced amplification of acoustic waves in a low Mach number granular flow

Lénaïc Bonneau, Tristan Catelin-Jullien, and B. Andreotti

Physique et Mécanique des Milieux Hétérogènes, UMR 7636, CNRS-ESPCI, 10 rue Vauquelin, 75231 Paris Cedex 05, France

(Received 10 November 2009; revised manuscript received 11 May 2010; published 30 July 2010)

We show experimentally that, contrary to ordinary fluids, low Mach number granular pipe flows are linearly unstable toward the emission of acoustic waves. Exponential amplification of the waves propagating in the direction opposite to the flow is directly demonstrated. We relate the observed instability to the friction of the grains on the pipe, which pumps energy from the mean flow to coherent elastic waves. We show that the most amplified wavelength is proportional to the ratio of the tube radius to the friction coefficient.

DOI: [10.1103/PhysRevE.82.011309](https://doi.org/10.1103/PhysRevE.82.011309)

PACS number(s): 45.70.-n, 47.20.-k, 47.57.Gc

I. INTRODUCTION

In standard fluid dynamics, the compressibility of viscous liquids is usually neglected when the flow velocity is much smaller than the speed of sound. However, the incompressibility condition is violated when the viscosity strongly increases with pressure [1], a characteristic optimally verified by cohesionless granular assemblies [2–4]. A phenomenon reported several times in the literature [5–7] provides a striking illustration of the possible coupling, at low Mach number, between mean flow and elastic deformations: contrary to an ordinary fluid flowing in a pipe, a loud sound is emitted during the discharge of a smooth silo filled with grain. Both the dynamic mechanism and the frequency selection have remained unexplained up to now. Based on the literature, one may invoke different possible sources of spontaneous vibrations. Resonant standing modes could be excited by the flow inside the granular column [5,7]. The hysteresis of friction could lead to a stick-slip motion [5,6]. Dynamical arching at the outlet [8] could be responsible for flow beating. The interaction between air and grains [9] could make the flow unsteady. A similar phenomenon was recently observed in microfluidic pipe flows of concentrated colloidal suspensions [10] and interpreted in terms of solvent permeation and effect of the confinement on shear thickening. Here, we propose an alternative explanation based on the amplification of acoustic waves by friction [11–13] that is supported by both experimental and theoretical results. We show that such a granular pipe flow presents a convective instability leading to exponentially growing acoustic waves and ultimately to nonlinear traveling waves.

II. EXPERIMENTAL SETUP

A. Experimental protocol

We have performed systematic experiments using 2 m long Polymethyl methacrylate (PMMA) tubes of radius R , ranging from 10 to 100 mm, to generate gravity driven homogeneous granular flows [see the schematic in Fig. 1(a)]. Thanks to the wall friction, the pressure and density fields are homogeneous, except in the vicinity of the outlet and of the free surface [14,15]. The setup presents significant differences with those previously used to study booming silos [5,6]. It is conceived to avoid spurious resonances due to the coupling with other parts of the system: the tube does not

rest on springs but is rigidly fixed to the laboratory wall and is filled continuously with granular material by a loading hopper during the entire experiment. Contrarily to [9], there is no air pressure difference across the silo. In that case, the experiment does not present any “ticking hourglass” effect, characterized by a frequency and a propagation speed two orders of magnitude lower than those measured in our experiment.

We use quartz sand grains of diameter $d=165 \pm 20 \mu\text{m}$ (from the mega-barchans of Sidi-Aghfinir, Atlantic Sahara; see the granulometry in [16]) and $d=325 \pm 45 \mu\text{m}$ [from the Pyla dune, Landes; see the granulometry in Fig. 1(b)]. In both cases, the sand is of Aeolian origin and has been sieved by the wind. The size distribution is sufficiently narrow [Fig. 1(b)] to avoid segregation in the experiment and the grains are rounded, due to the numerous collisions during the transport in saltation.

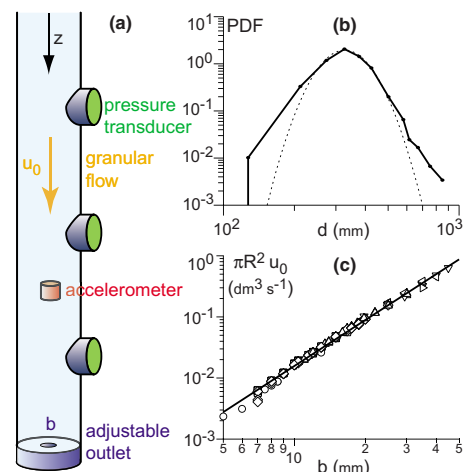


FIG. 1. (Color online) (a) Experimental setup. (b) Grain size distribution of Pyla silica sand: probability density function, weighted in mass, of the logarithm of the sand grain size d . The dotted line parabola is the best fit by a log-normal distribution, which gives the mean grain size, $d=325 \mu\text{m}$, with a $5 \mu\text{m}$ uncertainty. (c) Relation between the output flow-rate $\pi R^2 u_0$ and the outlet diameter b , measured for different tube radius: $R=8 \text{ mm}$ (\circ), $R=16 \text{ mm}$ (\square), $R=20 \text{ mm}$ (\diamond), $R=27 \text{ mm}$ (\triangle), $R=41 \text{ mm}$ (∇), $R=41 \text{ mm}$ (\triangleleft) and $R=46 \text{ mm}$ (\triangleright). The solid line is the best fit by the Beverloo law (Eq. (1)).

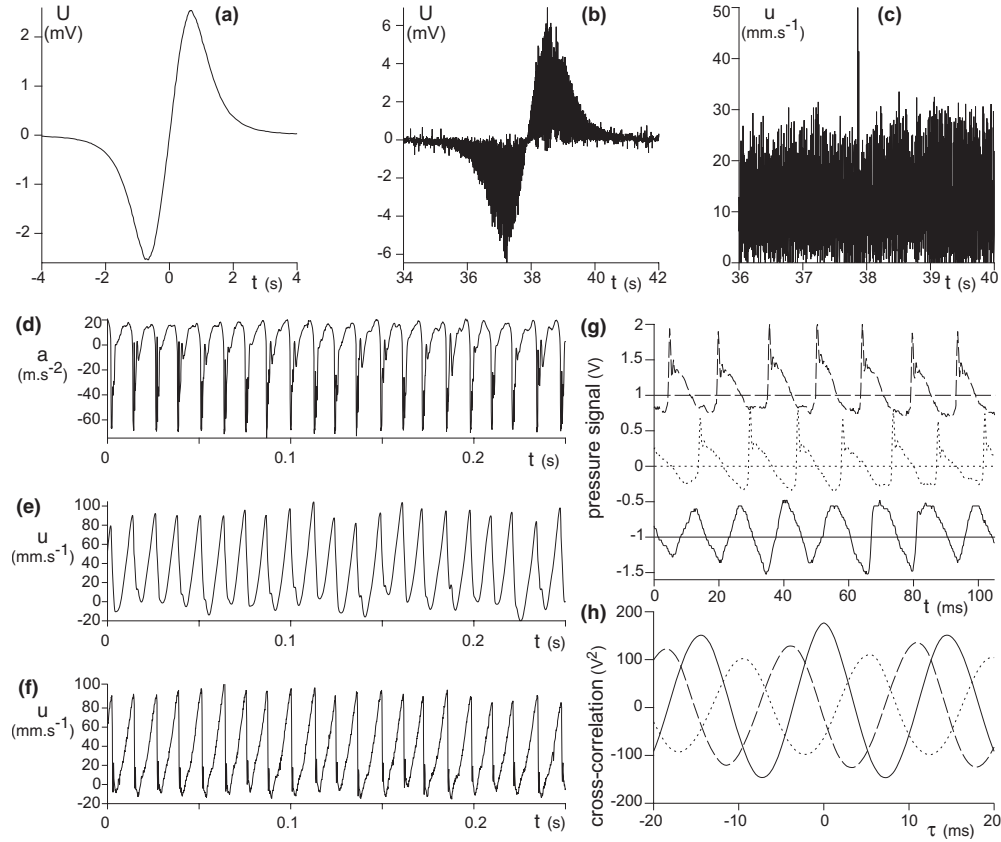


FIG. 2. Methods (a–c) Measurement of vibrations using a centimeter-scale alnico magnet embedded in the sand, on the axis of the silo. The raw signal recorded is the electromotive force $e = -\frac{d\Phi}{dt}$ induced in a coil wire-wound around the tube. Φ , the magnetic flux, is a function of the distance between the magnet and the coil. The magnet velocity signal reads $\frac{dz}{dt} = -e / \frac{d\Phi}{dz}$, where $\frac{d\Phi}{dz}$ is expressed as a function of Φ using a calibration signal. Φ is itself determined by integration of e . The signal cannot be used when the magnet is far from the coil, or right at its center. (a) Calibration signal recorded by induction of a magnet moving at a constant controlled velocity. (b) Signal obtained during a discharge. (c) Corresponding magnet velocity signal. (d–f) Comparison of the velocity signal measured with two independent methods. (d) Accelerometer signal. (e) Velocity signal measured by integrating the accelerometer signal. The constant of integration is fixed at u_0 . (f) Velocity signal measured using the magnet technique. (g–h) Correlation of pressure signals. (g) Three pressure signals recorded simultaneously. The signal in dotted line is measured at 33 cm above that in solid line and the signal in dashed line at 39 cm above that in blue. (h) Correlation of the three signals with the signal in solid line. The autocorrelation (solid line) gives the frequency f_m . The two cross-correlations (dotted and dashed lines) give the propagation time and thus the wave-speed c . The combination of the two measurements give the wave-number k_m .

B. Mean flow characteristics

In order to control the mean flow velocity u_0 , the bottom end of the tube is fitted by a PVC plug in which a cylindrical outlet is reamed. The hole diameter b is varied from $20d$ to $1.5R$. As shown in Fig. 1(c), the velocity u_0 is selected by b according to the Beverloo law [17],

$$\pi R^2 u_0 \approx 0.5g^{1/2} b^{5/2}, \quad (1)$$

and ranges from 1.5 to 150 mm s⁻¹. We have checked with scales that the output flow rate is not pulsed. The mean flow velocity u_0 is measured using three independent techniques:

(i) a colored intruder is introduced and the time taken to cross the silo is measured with a chronometer; (ii) after measurement, the silo is emptied and the sand level is measured as a function of time; (iii) the induction of a centimeter-scale magnet embedded in the sand into a coil wire-wound around the tube is analyzed (see Fig. 2).

These techniques give the same value of u_0 within error bars. Moreover, the motion of the grains touching the silo boundary is observed with a fast video camera (1000 images/s). The space-time diagram of Fig. 5(a) shows that the grains move downward with a velocity modulated around an average equal to u_0 , within measurement errors. Moreover, visualizing the granular free surface from the top of the silo, we could not detect any radial grain motion. We thus conclude that the mean velocity field is homogeneous in the section of the tube. This shear localization at the boundary originates from the fact that the interparticle effective friction is larger than that between the grains and the boundary.

C. Vibration measurement

During the discharge of the silo, coherent seismic waves are spontaneously emitted. As granular material is heterogeneous, it is important to use acoustic transducers much larger

than the grain size d , but smaller than the wavelength λ [18,19]. Indeed, the relative amplitude of the coherent effective medium response and of the multiscattered wave is directly proportional to the number of grains in contact with the transducer. We have used centimeter-scale sensors, which are in contact with $\approx 10^4$ grains. By comparison, in our series of experiments, the acoustic wavelength lies between 10 cm and 1 m.

The grain velocity fluctuations have been measured with three independent techniques:

- (i) the magnet technique described above (see Fig. 2).
- (ii) The signals of Bruel and Kjaer accelerometers of diameter 13 mm embedded in the granular flow are integrated in time (see Fig. 2). These piezoelectric transducers have a high sensitivity [500 mV/(m s⁻²)] and a high resolution of a fraction of nanometer at 100 Hz. Although the density of the transducers (7500 km/m³) is higher than that of silica (2650 km/m³), no significant relative motion with respect to the grains is observed.

(iii) The grains touching the boundary are imaged with a fast video camera. The velocity is then derived by cross-correlation between images.

Figure 2 shows that the Lagrangian signals obtained using an accelerometer and the induction of a magnet are very similar.

To perform the systematic experiments, we have fitted four piezoelectric sensors within the silo boundary (Fig. 1). In comparison to the accelerometers, they do not disturb the flow, but they are noisier and they do not have a flat frequency response (see Fig. 2). We have not used these signals to get information on the shape of the signal but to measure the frequency f_m , the wave-speed c and the wave-number $k_m=2\pi f_m/c$. We will detail below the procedure used to measure these quantities from the signal correlation functions.

III. CONVECTIVE LINEAR INSTABILITY

A. Upward seismic wave propagation

The different signals (acceleration, velocity, and pressure) recorded during the discharge of the silo show that granular matter vibrates periodically in time. Figure 3 shows typical signals measured using accelerometers. Just above the outlet, the signals are essentially low amplitude noises characterized by a broadband spectrum (Fig. 4). As a consequence, the vibration is not due to the dynamics close to the constriction used to control the flow rate. In other words, the acoustic emission does not result from dynamical arching at the outlet [8]. The region immediately above the outlet plays the role of a white noise source in the system. At a few tube diameters above the outlet, one observes the emergence of elastic waves at a well defined frequency f_m [Fig. 3(a)]. By definition, f_m is the inverse of the period, which is determined from the first maximum of the correlation function $\langle a(t)a(t+\tau) \rangle$ (Fig. 4). As the signals are quasiperiodic, this is much more precise than a measurement based on Fourier transform. The frequency is found to be constant over the whole tube. Moreover, it is independent of the length of the silo, so that the hypothesis of resonant standing modes can be re-

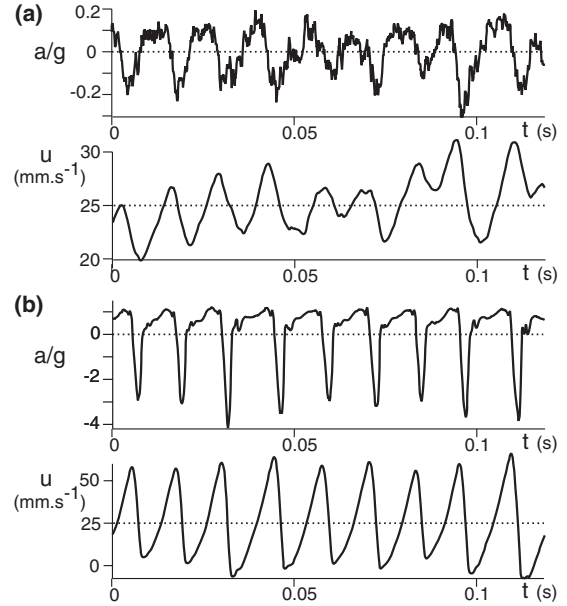


FIG. 3. (a) Typical acceleration a and velocity u signals (solid lines) measured in the bottom part of a tube of radius $R=32$ mm, for a mean flow velocity $u_0=25$ mm/s (dotted line). As expected for a linear instability, the signals present a well defined frequency and are roughly sinusoidal. (b) Sample of the signals measured in the upper part of the tube, in the fully developed nonlinear regime.

jected. The emitted frequency f_m does not depend strongly on the flow rate and on the tube radius and ranges from 60 to 90 Hz.

To characterize the propagation of these seismic waves, we have measured simultaneously the velocities of two magnets separated vertically by a distance z (see Fig. 2). From the maximum of the cross-correlation between the induction signals, one determines the time-lag t of an event followed between the two transducers. The silo is discharged using the same conditions for different values of z . The resulting curve between space and time, shown in Fig. 5(b), is linear. It shows that the spontaneous vibration is associated with propagative seismic waves. Moreover, these waves propagate exclusively in the direction opposite to the flow. The phenomenon is thus associated with a breaking of the symmetry between downward and upward propagation.

The slope of the curve $z(t)$ gives the propagation speed c . Like the frequency, c does not depend on the altitude in the silo, within error. To measure c systematically as a function of the flow rate and of the tube radius, we have used the signals received by the four pressure transducers arranged along the silo. Their phases, determined by cross-correlation, always point to waves propagating in the direction opposite to the flow [Fig. 5(b)]; no wave propagating upward in the silo has ever been observed. The wave velocity c is much larger than u_0 and ranges from 20 to 70 m/s when the tube radius and thus the pressure is varied. As expected for pressures on the order of 10^4 Pa, the wave speed c is much lower than that observed in a block of quartz (5600 m/s). This is a direct consequence of the contact geometry between grains, which leads to a low stiffness. The order of magnitude of c is

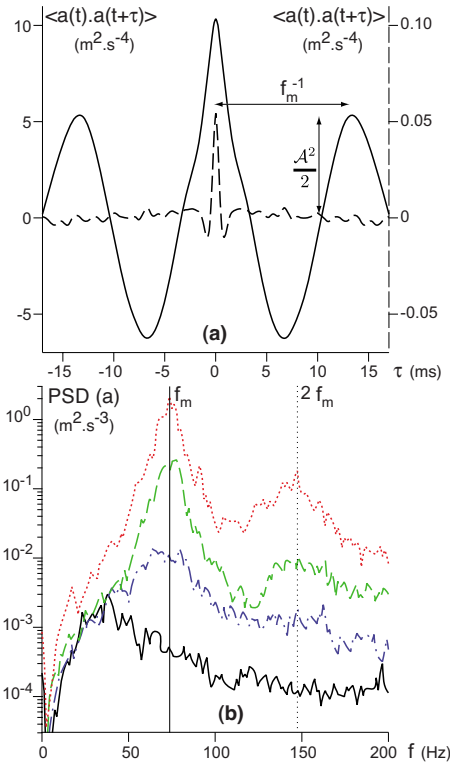


FIG. 4. (Color online) (a) Correlation of the accelerometer signal at 4 cm (dotted line, right axis) and 90 cm (solid line, left axis) above the outlet. The signal immediately above the outlet is a low amplitude noise. Higher in the tube, once the instability is developed, a well defined frequency f_m emerges. The first nontrivial correlation maximum allows the accurate measurement of the frequency f_m and the amplitude \mathcal{A} . (b) Power spectral density of the acceleration signal at 6 cm (solid black line), 42 cm (dotted-dashed blue line), 64 cm (dashed green line) and 146 cm (dotted red line) above the outlet. The vertical solid line shows the frequency f_m measured by correlation. The signal immediately above the outlet (solid line) is a low amplitude noise. In the linear regime (dotted-dashed line), the frequency f_m is selectively amplified. The growth rate is measured in this range of heights. Then, while the amplitude at f_m keeps growing, some harmonics appear (dashed and dotted lines).

consistent with that obtained when measuring the propagation of sound at the surface of a static granular layer [19].

B. Exponential amplification of seismic waves

Looking at the evolution of the signals from the outlet to the top of the tube, one observes a progressive increase of the peak to peak signal amplitude. As shown in Fig. 4, the wave amplitude \mathcal{A} is measured using the autocorrelation function of the acceleration signal,

$$\mathcal{A} = \sqrt{\langle 2a(t)a(t+1/f_m) \rangle}.$$

Note by contrast that the root mean square amplitude $\sqrt{\langle 2a(t)^2 \rangle}$ mixes the coherent signal and the residual noise and thus leads to a biased estimate of the amplitude. As for f_m , measurements of \mathcal{A} based on Fourier transform would be much less accurate than the correlation technique. Figure 6

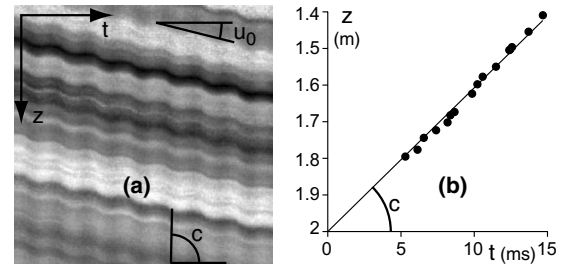


FIG. 5. (a) Space-time diagram showing the positions of the grains as a function of time. The grains in contact with the silo—a glass cylinder of radius $R=27$ mm in that case—are imaged with a fast video camera at mid height. One vertical line of the movie is plotted as a function of time. The mean velocity of these grains is equal, within 20%, to the bulk velocity u_0 . (b) Relation between space z and time lag t for a phase event followed by correlation of the magnetic induction signals measured at different z . The waves propagate upward at a velocity c much larger than u_0 .

shows that \mathcal{A} increases exponentially with height and saturates at a value \mathcal{A}_∞ , on the order of the gravity acceleration constant g . From a symmetry argument, one can write a Ginzburg-Landau equation of the form,

$$\frac{\partial \mathcal{A}}{\partial z} = -q_m \mathcal{A} \left(1 - \frac{\mathcal{A}^2}{\mathcal{A}_\infty^2} \right), \quad (2)$$

where q_m is the space amplification. The \mathcal{A}^3 term encodes the effect of the first nonlinearities. The solution of this equation takes the form,

$$\mathcal{A} = \frac{\mathcal{A}_\infty}{\sqrt{1 + \eta \exp(2q_m z)}}, \quad (3)$$

where η reflects the noise level at the output. Figure 6 shows that it nicely fits the amplitude measured experimentally.

In the upper part of the tube, the signals progressively distort, a phenomenon associated with the emergence of harmonics in the Fourier spectrum [Fig. 4(b)]. These features, together with the saturation of the signal amplitude, are characteristic of nonlinear acoustic effects. As shown in Fig. 3(b), the acoustic waves tend to form shocks. The vertical axis z

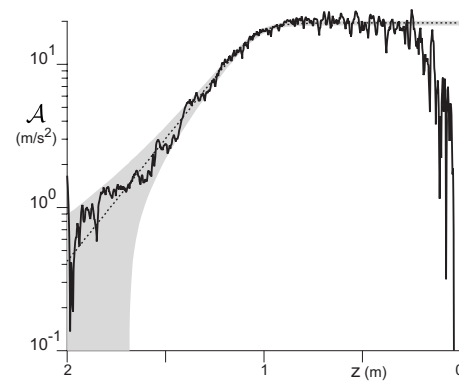


FIG. 6. Amplitude \mathcal{A} of the acceleration signal as a function of the vertical coordinate z . The dotted line shows the best fit by the amplitude Eq. (3).

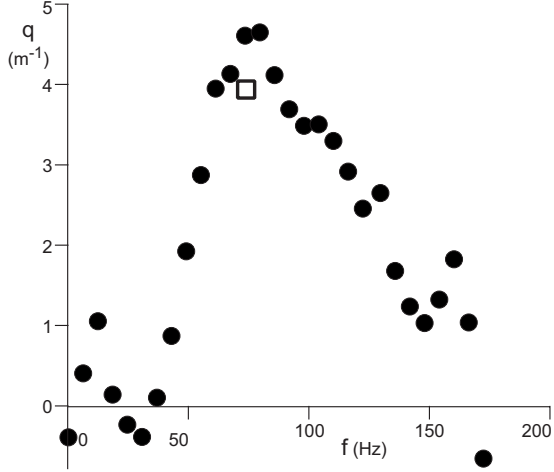


FIG. 7. Spatial growth rate q as a function of frequency f (●). The square shows the value of q_m determined from Fig. 6. The emission frequency $f_m \approx 75$ Hz coincides with the maximum of the growth rate. Same conditions as in Fig. 3.

is, by convention, oriented downward. The velocity u shown in Fig. 3(b) is thus positive, with an average value equal to u_0 . Most of the time, the grains are accelerated downward with an acceleration on the order of g . This period of time during which the granular medium is decompressed is followed by a strong deceleration ($a < 0$) after which the grains come to rest. This sequence is characteristic of stop and go waves. This is confirmed by direct visualization of the space-time diagram of Fig. 5(a).

C. Convective linear instability

The exponential amplification, together with the upward propagation of unstable modes, is the signature of a convective linear instability [20]. To confirm this scenario, we have analyzed the acceleration fluctuation spectrum at different heights [Fig. 4(b)]. In the bottom part of the tube i.e., in the region of exponential amplification, a narrow range of frequencies around f_m is amplified. We have determined the spatial growth rate $q(f)$ of each mode by fitting the curves of the Fourier amplitude as a function of space by an exponential. The dispersion relation $q(f)$ is plotted in Fig. 7. It is positive in a frequency band and presents a maximum that nicely corresponds to the spontaneous emission frequency f_m . This confirms the scenario of a convective linear instability: the random fluctuations around the outlet are selectively amplified around f_m during wave propagation.

IV. AMPLIFICATION MECHANISM

A. Simple one-dimensional (1D) model

As the emitted wavelength is much larger than the tube radius, the system can be thought of as a 1D compressible system. This constitutes the so-called Janssen approximation [21]. We introduce the density ρ , the velocity u and the axial stress P , averaged over the section of the tube [Fig. 8(a)]. The continuity and momentum equations can be written under the form,

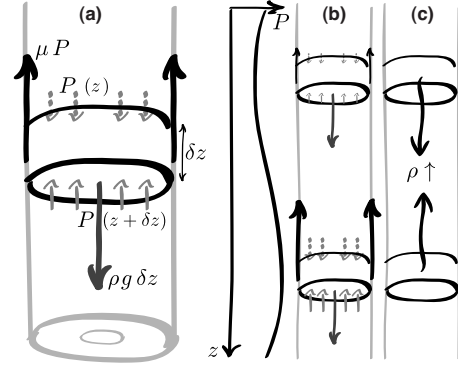


FIG. 8. Schematic of the amplification of acoustic waves by friction. (a) On average, the weight of the granular column is balanced by the friction on the boundary of the silo. (b) During the propagation of an acoustic wave in the column, the high pressure regions are submitted to a greater friction than the low-pressure ones. For small wave amplitudes, the grain velocity remains oriented downward so that the friction everywhere is oriented upward. (c) This results into an unbalanced force that tends to compress the grain region, noted $\rho \uparrow$, between the high pressure and the low-pressure regions immediately above. Due to inertia, this compression requires time, during which the wave propagates. If the wave propagates upward, the high pressures are reinforced by friction and low pressures are lowered, amplifying the acoustic wave.

$$\dot{\rho} + \rho \frac{\partial u}{\partial z} = 0 \quad \text{and} \quad \rho a = \rho \dot{u} = \rho g - \frac{\partial P}{\partial z} - \frac{2\mu}{R} P, \quad (4)$$

where μ is the product of the grain-tube friction coefficient by the ratio of radial to axial stress. Due to the mean flow u_0 , the local velocity is always downward so that the wall friction force is oriented upward (Fig. 8). On the average, the grain weight is balanced by this friction [Fig. 8(a)]. At equilibrium, in a long tube, the axial stress is thus a constant controlled by the tube radius,

$$P_0 = \frac{\rho g R}{2\mu}. \quad (5)$$

As is standard for solids or liquids, we define the speed of compression waves as

$$c_0^2 = \frac{\partial P}{\partial \rho}. \quad (6)$$

Importantly, c_0 may depend on the pressure P_0 . Note also that this speed of sound is defined in the absence of friction, from the constitutive relation $P(\rho)$ of the material. We denote by ρ_1 , u_1 , and P_1 the disturbances of density, velocity, and axial stress associated to the waves. We consider the limit of a low Mach number ($\mathcal{M} = u_0/c_0 \ll 1$), for which convection can be neglected: $\dot{u} \approx \partial_t u$ and $\dot{\rho} \approx \partial_t \rho$. Note that this assumption is not necessary in the reference frame of the moving sand. The continuity equation, the dynamical equation and the constitutive relation can then be linearized,

$$\frac{\partial \rho_1}{\partial t} = -\rho_0 \frac{\partial u_1}{\partial z}, \quad (7)$$

$$\rho_0 \frac{\partial u_1}{\partial t} = \rho_1 g - \frac{\partial P_1}{\partial z} - \frac{2\mu}{R} P_1, \quad (8)$$

$$P_1 = c_0^2 \rho_1. \quad (9)$$

This equation set can be rewritten as a wave equation for any of the three variables,

$$\frac{\partial^2 u_1}{\partial t^2} = c_0^2 \left[\frac{\partial^2 u_1}{\partial z^2} + \frac{2}{\ell} \frac{\partial u_1}{\partial z} \right]. \quad (10)$$

where the length ℓ is given by

$$\ell = \left(\frac{\mu}{R} - \frac{g}{2c_0^2} \right)^{-1} \approx \frac{R}{\mu}. \quad (11)$$

In this expression, the gravity term is negligible when the tube radius is much smaller than, typically, 10 m. When ℓ tends to infinity, one recovers the standard Helmholtz equation: acoustic waves can propagate in both directions at the velocity c_0 . The unusual term in ℓ^{-1} is due to friction and breaks the symmetry between upward and downward propagation. It is nonconservative and operates in quadrature with respect to the restoring force. We will see that this term is responsible for the instability.

B. Dispersion relation

As the steady state is homogeneous in space and time, the solutions of the linearized equations are superpositions of Fourier modes of the form $\exp[j(\omega t + kz)]$, where both ω and k can *a priori* be complex. The dispersion relation takes the form,

$$\omega^2 = c_0^2 \left(k^2 - j \frac{2}{\ell} k \right). \quad (12)$$

As we look for the existence of propagative modes growing in space [20], we consider a real frequency ω and a complex wave-number $k = \kappa + jq$. $\kappa = 2\pi/\lambda$ is the real wave number and q the space growth rate. We aim to determine if a seismic wave at the frequency ω amplifies or not during its propagation. The dispersion relation simplifies into,

$$q = \frac{1}{\ell} \quad \text{and} \quad \kappa = \pm \sqrt{\frac{\omega^2}{c_0^2} - \frac{1}{\ell^2}}. \quad (13)$$

The wave propagating upward in the tube ($\kappa > 0$) are thus amplified exponentially ($q > 0$) over a length ℓ . This dispersion relation predicts that all the unstable modes are propagating upward in the tube. The instability is thus convective. Moreover, there exists a critical frequency c_0/ℓ below which the waves do not propagate at all.

Let us reformulate this result in terms of qualitative dynamic mechanisms. Consider an elastic wave. A high pressure region results in friction larger than average so that it is accelerated upward [Fig. 8(b)]. Conversely, the low-pressure region immediately above it is accelerated downward. The region in between therefore gets compressed [Fig. 8(c)]. Due to inertia, there is a time delay between the application of the friction forces and the resulting compression, during which

the wave propagates. Considering a pressure wave propagating downward the tube, compression takes place in the low-pressure region and leads to a spatial attenuation. Conversely, for upward propagating waves, the compression reinforces the high pressure, which results in acoustic amplification. This constitutes a very robust amplification mechanism, insensitive to the details in the modeling equations. The key point lies in the polarization of the friction force. When one emits a wave in a static silo, the friction is everywhere opposed to the velocity of the grains at the boundary. The wave is thus attenuated. If one adds a mean downward velocity, the friction force remains orientated upward as long as the wave does not reach an amplitude such that the grains locally move up. The friction then becomes a source of acoustic amplification.

C. Wavelength selection

If the wall friction is responsible for wave amplification, it does not explain the observed wavelength selection. Indeed all the frequencies above c_0/ℓ are equally amplified by friction. Wave damping is the most obvious mechanism missing in the previous description. This dissipation is mostly localized in the region of contact between grains and can result from either the viscoelasticity of microcontacts, the linear viscous loss due to liquid films trapped in grain surface asperities, or to solid friction [22,23]. For the sake of simplicity, we introduce a constant bulk viscosity ν in the constitutive relation written at the linear order, which modifies into

$$P_1 = c_0^2 \rho_1 + \nu \frac{\partial \rho_1}{\partial t}. \quad (14)$$

We consider again a Fourier mode of the form $\exp[j(\omega t + kz)]$. The constitutive relation then gives

$$P_1 = (c_0^2 + \nu j \omega) \rho_1. \quad (15)$$

Neglecting the gravity term, the mass and momentum conservation Eqs. (7) and (8) lead to the relations,

$$j \omega \rho_1 = -\rho_0 j k u_1, \quad (16)$$

$$\rho_0 j \omega u_1 = - \left(j k + \frac{2}{\ell} \right) P_1. \quad (17)$$

Altogether, we obtain the modified dispersion relation,

$$\frac{\omega^2}{c_0^2 + j \nu \omega} = k^2 - j \frac{2}{\ell} k. \quad (18)$$

We now make the equations dimensionless. The typical length-scale is ℓ ; the typical time scale is ℓ/c_0 . We define the dimensionless wave-number $\tilde{k} = k\ell$ and the dimensionless frequency $\tilde{\omega} = \frac{\ell \omega}{c_0}$. There is a single nondimensional number, the quality factor \mathcal{Q} built by making ν nondimensional using the speed of sound c_0 and the length-scale ℓ ,

$$\mathcal{Q} = \frac{c_0 \ell}{\nu}. \quad (19)$$

The dispersion relation can then be rewritten as

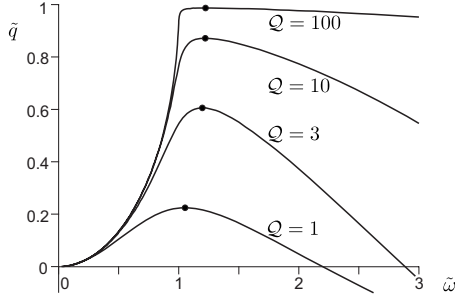


FIG. 9. Theoretical dispersion relation: nondimensional growth rate \tilde{q} as a function of $\tilde{\omega}$ for different quality factors Q .

$$\frac{\tilde{\omega}^2}{1 + jQ^{-1}\tilde{\omega}} = \tilde{k}^2 - 2j\tilde{k}. \quad (20)$$

As before, we consider a real frequency $\tilde{\omega}$ and a complex wave number $\tilde{k} = \tilde{\kappa} + j\tilde{q}$. The dispersion relation can be expressed by two coupled equations that can be easily solved,

$$\tilde{\kappa}^2 - \tilde{q}^2 + 2\tilde{q} = \frac{\tilde{\omega}^2}{1 + Q^{-2}\tilde{\omega}^2}, \quad (21)$$

$$\tilde{q} = 1 - \frac{\tilde{\omega}^3}{2Q\tilde{\kappa}(1 + Q^{-2}\tilde{\omega}^2)}. \quad (22)$$

Figure 9 shows the relation between the growth rate and the frequency for different quality factors. One observes that the introduction of acoustic dissipation allows the theoretical recovery of frequency selection. Surprisingly, the frequency and the wavelength selected do not depend strongly on the quality factor, when the latter is larger than one.

At low $\tilde{\omega}$, both the growth rate \tilde{q} and the wave-number \tilde{k} tend to 0. In the limit of large Q , the second equation leads to the asymptotic behavior $\tilde{\kappa} \approx \tilde{\omega}^3/(2Q)$. Then, the first equation gives: $\tilde{q} \approx \tilde{\omega}^2/2$. In the limit where the damping can be neglected ($Q = \infty$), one recovers the existence of a threshold frequency below which the waves do not propagate.

Still in the limit of large Q , at large $\tilde{\omega}$, one recovers the undisturbed dispersion relation $\tilde{\kappa} \approx \tilde{\omega}$. The second equation then gives $\tilde{q} \approx 1 - \tilde{\omega}^2/(2Q)$. As the acoustic damping is more efficient at large wavelength, it leads to a decrease of the growth rate \tilde{q} with $\tilde{\omega}$.

The maximum growth rate is thus selected on one side by the forbidden band of frequencies and on the other side by attenuation of large frequencies. In the limit of large Q , the frequency, the wavelength and the growth rate selected are independent of Q and read

$$q_m = \frac{1}{\ell}, \quad \kappa_m = \frac{1}{\sqrt{2}\ell}, \quad \omega = \sqrt{\frac{3}{2}} \frac{c_0}{\ell}. \quad (23)$$

V. PARAMETRIC STUDY OF THE INSTABILITY

We have seen that the minimal model derived under the Janssen approximation predicts a convective instability, with a selective amplification of upward propagating waves (Fig.

5) and a dispersion relation resembling that observed experimentally (Figs. 7 and 9). We emphasize that this model is not supposed to describe the instability in all its details, but to point to robust dynamic mechanisms. In the model, the destabilizing mechanism is the wall friction; the stabilizing one is acoustic damping. To validate the origin of the instability, two predictions can be tested experimentally: the effect of the friction coefficient between the grain and the wall on the instability and the proportionality of the selected wavelength on the tube radius.

A. Influence of the friction coefficient

To perform the first of these two tests, we have changed the friction coefficient between the tube and the grains, without changing any other parameter in the system. We have coated a tube with polytetrafluoroethylene (PTFE). When used as a lubricant, PTFE, which is most well known by the DuPont brand name Teflon, reduces friction, wear and energy consumption at the contact between solids.

To measure the friction coefficient between grains and PMMA, we have progressively inclined a tube in which a small sand puddle is settled. The angle at which the sand material starts flowing coherently is measured within a degree. For the interface between pyla sand and PMMA, we find a static friction coefficient $\mu_s = 0.48 \pm 0.03$. Once the tube is coated with PTFE, the static friction coefficient of sand is reduced by a factor of two: $\mu_s = 0.23 \pm 0.05$. Figure 10 shows that the acoustic emission obtained is very strongly affected by the PTFE coating: the vibration amplitude is reduced by a factor of ten. The sound power emitted in the air by the vibration of the free surface is reduced by two orders of magnitude so that it can no longer be heard. A first qualitative conclusion can be reached: when the friction is decreased without changing either the grains or their flow rate nor the acoustic properties of the silo, the instability is strongly reduced. More quantitatively, the amplification rate observed with the PTFE coating ($q = 3.2 \pm 1 \text{ m}^{-1}$) is reduced by a factor of 2, when compared to the reference case ($q = 7.3 \pm 1 \text{ m}^{-1}$). We have also used smooth spherical silica beads flowing in a noncoated tube, with the same physical properties as the pyla sand except their shape ($\mu_s = 0.34 \pm 0.03$). Figure 10 shows the frequencies f_m obtained in these three cases: $f_m \approx 76 \pm 3 \text{ Hz}$ for sand on PMMA, $f_m \approx 51 \pm 5 \text{ Hz}$ for glass beads on PMMA and $f_m \approx 33 \pm 5 \text{ Hz}$ for sand on PTFE. In conclusion, the emitted frequency f_m increases with coefficient of friction between the grains and the tube, as predicted by the model.

B. Wavelength scaling law

Figure 11 shows the relation between the measured wavelength λ_m and the tube radius R for comparable friction coefficients. As predicted by the model, λ_m is proportional to R . Figure 12 shows the wave number rescaled by the tube radius $k_m R$. Although scattered, the values of $k_m R$ coincides with $\mu/\sqrt{2}$ (between 0.2 to 0.3) within uncertainties. Beyond the scaling law, we thus have semiquantitative agreement with the prediction of the wavelength of maximum amplification.

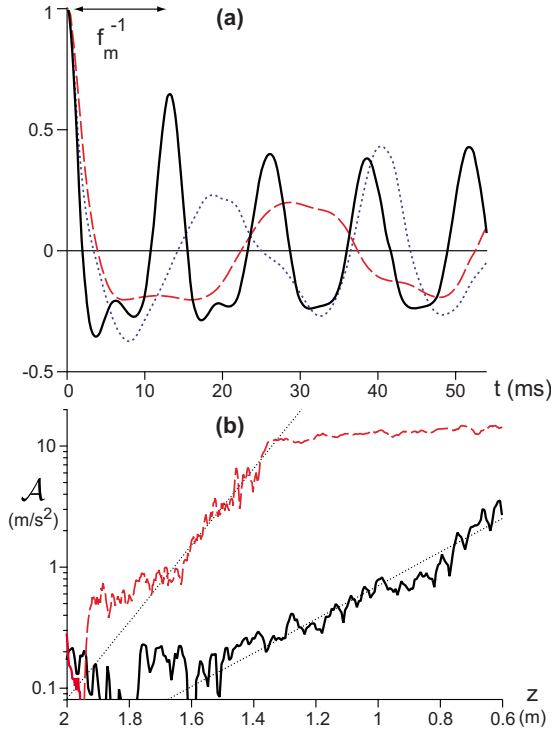


FIG. 10. (Color online) Influence of friction on the spatial growth of the vibration amplitude. (a) Autocorrelation of the accelerometer signal at $z=0.5$ m, for a tube radius $R=27$ mm and a mean velocity $u_0=39$ mm/s. The solid line shows the reference case (Pyla silica sand). When the friction between the grains and the silo is reduced, either by using silica beads (dotted line) or by coating the silo with polytetrafluoroethylene (PTFE) (dashed red line) the frequency f_m decreases. (b) Amplitude of the acceleration signal as a function of depth, with (solid line) and without (dashed red line) coating the silo with polytetrafluoroethylene (PTFE). The tube radius is $R=27$ mm and the mean velocity $u_0=39$ mm/s. When the friction is decreased, without any other change, the amplification rate (dotted line) and the frequency get strongly reduced (by a factor between 2 and 2.5).

To go further in the comparison between model and experiment, one needs to calibrate the dependance of the friction coefficient μ with the flow velocity u_0 . In previous studies [14,15], this measurement has been performed using a strain gauge sensor mounted on a piston which is kept at a distance from the tube larger than 0 but smaller than $\sim d/3$. With grains of few hundred microns and velocities up to 10 cm/s, we were unable to build such a calibration apparatus. Thus, we examine our results using the curves $\mu(u_0)$ published in the literature for grains larger than a millimeter. It has been systematically observed by [14,15] that μ increases as the logarithm of the velocity [Fig. 12(b)]. We also observe in Fig. 11(a) a trend of $k_m R$ to increase slowly with the logarithm of u_0/d . In conclusion, we have shown that λ_m is proportional to R as expected, and that $k_m R$ is consistent with $\mu/\sqrt{2}$. Further work is needed to clarify the origin of the dependence with respect to the flow velocity. Figure 13 reports measurements of the frequency f_m and of the wave-speed c . While the simplest mean field calculation [24] leads

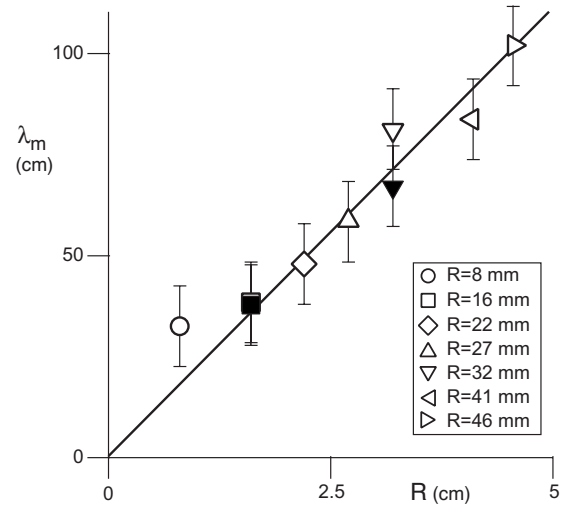


FIG. 11. Measured wavelength λ_m as a function of the tube radius R , for $u_0/d=100 \pm 20$ s⁻¹. Black: $d=165$ μ m. White: $d=325$ μ m.

to $c=\omega/k \propto R^{1/6}$, our measurements show a much faster increase with R [Fig. 13(b)] that remains unexplained.

VI. CONCLUSION

In conclusion, our experiment has allowed us to establish several facts concerning the instability of a granular pipe flow:

- (i) the spontaneous emergence of vibrations is related to elastic waves which propagate exclusively upward, in the direction opposite to the flow;
- (ii) these waves are amplified

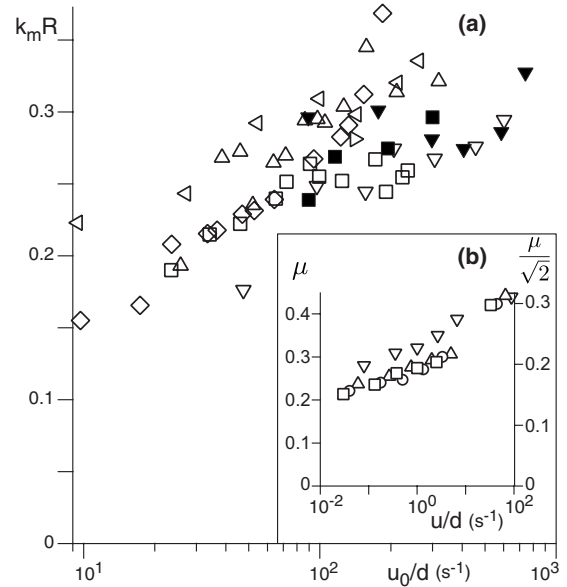


FIG. 12. (a) Measured wave number k_m rescaled by the tube radius R , as a function of u_0/d . Same symbols as in Fig. 11. (b) Relation between the coefficient μ and u/d obtained experimentally by Bertho *et al.* [15] for glass beads flowing in a glass tube. The data obtained for different grain size are represented: $d=1.5$ mm (∇), $d=2$ mm (\triangle), $d=3$ mm (\circ) and $d=4$ mm (\square).

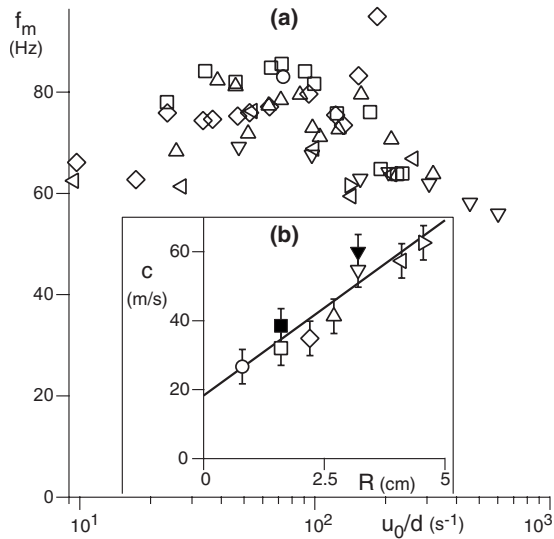


FIG. 13. (a) Measured frequency f_m as a function of u_0/d . (b) Wave velocity c as a function of the tube radius R , for $u_0/d = 100 \pm 20$ s^{-1} . Same symbols as in Fig. 11.

exponentially in the course of their propagation; (iii) the frequency selected corresponds to the most amplified mode of a linear convective instability; (iv) the instability can be strongly reduced by decreasing the friction between the grains and the silo; (v) for a given friction, the wavelength scales with the tube radius; (vi) the elastic waves tend to form shocks and their amplitude saturates as they become stop-and-go waves. This series of observations is consistent with the robust dynamic mechanism exhibited here: friction selectively amplifies waves propagating in the direction opposite to the flow. We have proposed a minimal model which includes four basic ingredients:

(a) It takes into account compressibility, even though the Mach number is small; otherwise, there would be no wave (i).

(b) The friction force exerted by the wall breaks the up/down symmetry, since it is exerted in the direction opposite to the total grain velocity; otherwise, one could not explain the observed symmetry breaking (i).

(c) The friction force increases with pressure; otherwise, the waves would not be coupled to the mean flow and would not be amplified (ii).

(d) Elastic waves are damped; otherwise, no frequency selection would occur (iii) and the nonlinear waves would break (vi).

Any other model verifying these properties would reproduce the set of observations (i-v). The weakness of the minimal model presented here lies in the Janssen assumption, which should be replaced in future studies by a derivation of normal modes in a full three-dimensional (3D) viscoelastic continuous model (see for instance [13]). A second possible

improvement is the calibration of the mechanical properties (elasticity, bulk damping, friction on the boundary) in the vicinity of the jamming transition, for the sake of quantitative comparison between model and experiment. Third, to take into account nonlinearities, the increase of the speed of sound with pressure will have to be taken into account. As waves in high pressure zones propagate faster than in low-pressure ones, the acoustic waves tend to form shocks and the second viscosity prevents breaking. Surprisingly, we did not observe significant changes of propagation speed between the linear and nonlinear regimes. A better space resolution will be needed to quantify the dependence of the wave speed on its amplitude.

Within a wider perspective, this paper illustrates a consequence of the frictional behavior of granular matter, i.e., the dependence of the deviatoric stresses on normal stresses. Contrary to a constant viscosity liquid, elastic and plastic modes of deformation are then coupled by pressure, even at low Mach number, a property which leads to instabilities [1]. The convective linear instability reported here can be associated to two independent characteristics. First, acoustic waves are guided along the tube. Second, acoustic waves traveling parallel to the tube are amplified by friction. It has been shown theoretically that elastic waves can be amplified when they are reflected on a frictional interface [11,12]. One thus expects a similar instability in all situations where an elastic wave guide is bounded by a frictional interface. We have recently shown that this is the principle of booming avalanches [13]. Just like the system investigated here, we have demonstrated that elastic waves propagating in the direction opposite to the avalanche are selectively amplified in space. The major difference lies in the wave guide geometry. During the silo discharge, the granular flow is surrounded by the cylindrical shear band, which acts as an amplifying acoustic mirror. By contrast, a booming avalanche is separated from the static part of the dune by a planar shear band whereas the free surface acts as a simple reflector. The experiment presented here can thus be thought of as a surrogate of booming avalanche [25].

Finally, we emphasize that the dynamic mechanism investigated here differs fundamentally from a passive resonator, which accumulates energy because resonant modes are not propagative. On the contrary, the dynamic mechanism evident here is a true amplification of guided propagative modes, with the energy being pumped from gravity, driving the flow, resulting in coherent acoustic energy.

ACKNOWLEDGMENTS

We thank D. Pradal and J. Lanuza for their technical assistance and E. Clément for his helpful advice. This work has benefited from the financial support of the Agence Nationale de la Recherche, grant ‘Zephyr’ (Grant No. ERCS07_18).

- [1] A. Furukawa and H. Tanaka, *Nature (London)* **443**, 434 (2006).
- [2] GDR Midi, *Eur. Phys. J. E* **14**, 341 (2004).
- [3] B. Andreotti, *EPL* **79**, 34001 (2007).
- [4] P. Jop, Y. Forterre, and O. Pouliquen, *Nature (London)* **441**, 727 (2006).
- [5] B. K. Muite, S. F. Quinn, S. Sundaresan, and K. K. Rao, *Powder Technol.* **145**, 190 (2004).
- [6] M. L. Dhoriyani, K. K. Jonnalagadda, R. K. Kandikatla, and K. K. Rao, *Powder Technol.* **167**, 55 (2006).
- [7] K. Wilde, M. Rucka, and J. Tejchman, *Powder Technol.* **186**, 113 (2008).
- [8] G. W. Baxter, R. P. Behringer, T. Fagert, and G. A. Johnson, *Phys. Rev. Lett.* **62**, 2825 (1989).
- [9] Y. Bertho *et al.*, *J. Fluid Mech.* **459**, 317 (2002).
- [10] L. Isa, R. Besseling, A. N. Morozov, and W. C. K. Poon, *Phys. Rev. Lett.* **102**, 058302 (2009).
- [11] M. Nosonovsky and G. G. Adams, *Int. J. Eng. Sci.* **39**, 1257 (2001).
- [12] C. Caroli and B. Velický, *Phys. Rev. E* **67**, 061301 (2003).
- [13] B. Andreotti and L. Bonneau, *Phys. Rev. Lett.* **103**, 238001 (2009).
- [14] G. Ovarlez, C. Fond, and E. Clément, *Phys. Rev. E* **67**, 060302(R) (2003).
- [15] Y. Bertho *et al.*, *EPL* **67**, 955 (2004).
- [16] H. Elbelrhiti, B. Andreotti, and P. Claudin, *J. Geophys. Res.* **113**, F02S15 (2008).
- [17] W. A. Beverloo, H. A. Leniger, and J. van de Velde, *Chem. Eng. Sci.* **15**, 260 (1961).
- [18] X. Jia, C. Caroli, and B. Velický, *Phys. Rev. Lett.* **82**, 1863 (1999).
- [19] L. Bonneau, B. Andreotti, and E. Clément, *Phys. Rev. Lett.* **101**, 118001 (2008).
- [20] P. Huerre and P. P. Monkewitz, *Annu. Rev. Fluid Mech.* **22**, 473 (1990).
- [21] H. A. Janssen, *Z. Ver. Dtsch. Ing.* **39**, 1045 (1895).
- [22] T. Baumberger, P. Berthoud, and C. Caroli, *Phys. Rev. B* **60**, 3928 (1999).
- [23] Th. Brunet, X. Jia, and P. Mills, *Phys. Rev. Lett.* **101**, 138001 (2008).
- [24] K. Walton, *J. Mech. Phys. Solids* **35**, 213 (1987).
- [25] B. Andreotti, *Phys. Rev. Lett.* **93**, 238001 (2004).